Assessment of proton radiation-induced charge transfer inefficiency in the CCD273 detector for the Euclid Dark Energy Mission

Conference or Workshop Item

Assessment of proton radiation-induced charge transfer inefficiency in the CCD273 detector for the Euclid Dark Energy Mission

J. P. D. Gow[a], N. J. Murray[a], D. J. Hall[a], A. S. Clarke[a], D. Burt[b], J. Endicott[b], A. D. Holland[a]
[a]e2v centre for electronic imaging, The Open University, DPS, Milton Keynes, MK7 6AA, UK
[b]e2v technologies plc, 106 Waterhouse Lane, Chelmsford, Essex, CM1 2QU, UK

ABSTRACT

Euclid is a medium class mission selected for launch in 2019, with a primary goal to study the dark universe using the weak lensing and baryonic acoustic oscillations techniques. Weak lensing depends on accurate shape measurements, therefore it is beneficial that the effects of radiation-induced charge transfer inefficiency (CTI) in the Euclid CCD over the six year mission are understood and minimised. This paper describes the initial evaluation of the tolerance to radiation induced charge transfer inefficiency (CTI) of the CCD273 produced by e2v technologies plc, making comparisons with the previous CCD selected for Euclid the CCD203. The CCD273 benefits from the inclusion of a charge injection structure for trap suppression and a reduction in the register channel width. The improvement in tolerance to radiation induced serial CTI achieved by reducing the channel width from 50 μm to 20 μm was measured experimentally to be a factor of 1.7, which compares well to a factor of 1.9 found using a charge volume model.

Keywords: CCD, Euclid, proton radiation damage, n-channel, charge transfer efficiency

1. INTRODUCTION

It has been understood since the 1930's that ordinary baryonic particles account for less than 17% of the total amount of matter in the universe[1], leading to the speculation into the existence of "dark matter" which is undetectable using traditional observation techniques. Light from distant galaxies will be, from the point of view of the observer, bent around massive intervening objects, resulting in a change in the galaxies ellipticity. These objects are referred to as gravitational lenses and the effect as gravitational lensing[2] an example of which is illustrated in Figure 1[3], observations can be used to measure the mass of the gravitational lens. During the late 1980's and early 90's the weak lensing (WL) technique[4-5] was developed where the change in ellipticity of galaxies is measured to the order of a few percent. This requires multiple galaxies and accurate shape measurement to calculate the amount and distribution of intervening matter.

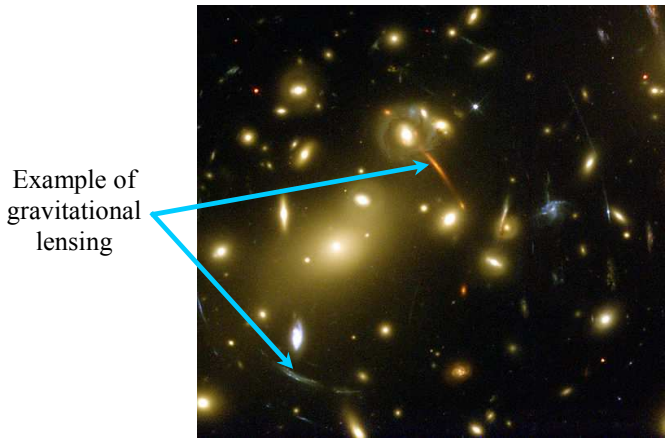

Figure 1. Galaxy cluster Abell 2218 captured by Hubble in 1999[7].

*j.p.d.gow@open.ac.uk; phone +44 (0)1908 332194; fax +44 (0)1908 655667; www.open.ac.uk/cei

One of the advantages of performing WL measurements from a space based telescope is the avoidance of atmospheric distortions allowing for the precision photometry required to analyse background galaxies[6-7]. The Euclid mission[8] was proposed, as part of the European Space Agency (ESA) Cosmic Visions programme, to investigate the history of the dark universe. Euclid was selected in October 2011 as the second M-class mission for launch in 2019 and will make use a combination of several techniques including WL[9] and Baryonic Oscillations[10]. The payload consists of a single telescope and the visible imager (VIS)[11], for which this work has been performed, and the near-IR photo-spectrometer[12] instruments.

The baseline CCD imager for the Euclid VIS instrument was originally the e2v technologies CCD203[8], a four phase 4k × 4k device with 12 µm square pixels illustrated in Figure 2, previously flown onboard the Solar Dynamics Observatory launched in 2010. The first radiation damage assessment performed for the CCDs in the VIS instrument, funded by ESA, was made using the CCD204; further details on this work can be found in references 13 to 15. The CCD204, illustrated in Figure 3, was produced using the same pixel and register structure as the CCD203 but with the inclusion of a charge injection structure. The CCD204 was mounted onto the larger CCD203 package as these were available during device assembly.

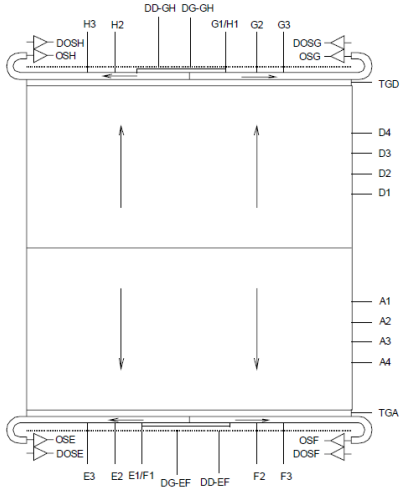

Figure 2. Schematic of the e2v technologies CCD203-82.

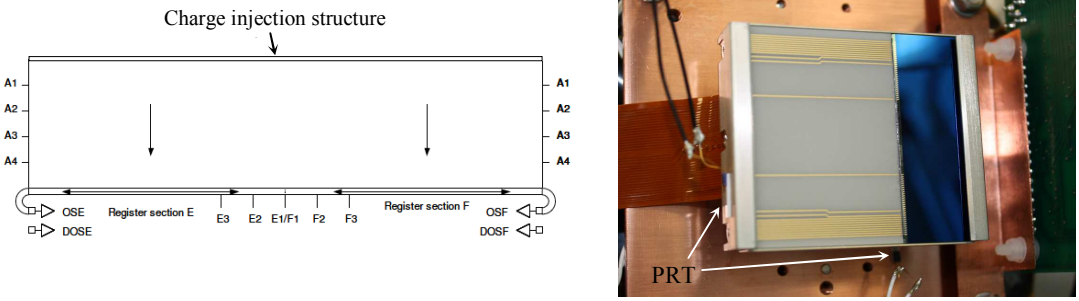

Figure 3. Schematic and photograph of the e2v technologies CCD204-22, the photograph shows the CCD204 mounted onto a copper cold bench as part of the CEI test camera.

The serial register of the CCD203/CCD204 was designed to allow on-chip pixel binning to be performed, resulting in a channel width of 50 µm. Models of the serial register developed as part of the CCD204 radiation damage assessment indicated a charge dependant improvement in CTI with decreased register volume[14] and as Euclid does not require on-chip binning it was decided to reduce the width, and hence volume, of the serial register. The inclusion of a charge injection structure was also recommended, having demonstrated high levels of parallel CTI recovery[13]. Discussion

between e2v technologies plc, ESA and the Euclid-VIS consortium led to the creation of a custom four phase 4k × 4k CCD with 12 µm square pixels, designated CCD273[16] and illustrated in Figure 4. The CCD273 incorporates a charge injection structure (taking the place of the central 4 pixel rows), a register width of 20 µm and a low noise output stage, as used in the CCD231. Details on the CCD203, CCD204 and CCD273 are given in Table 1.

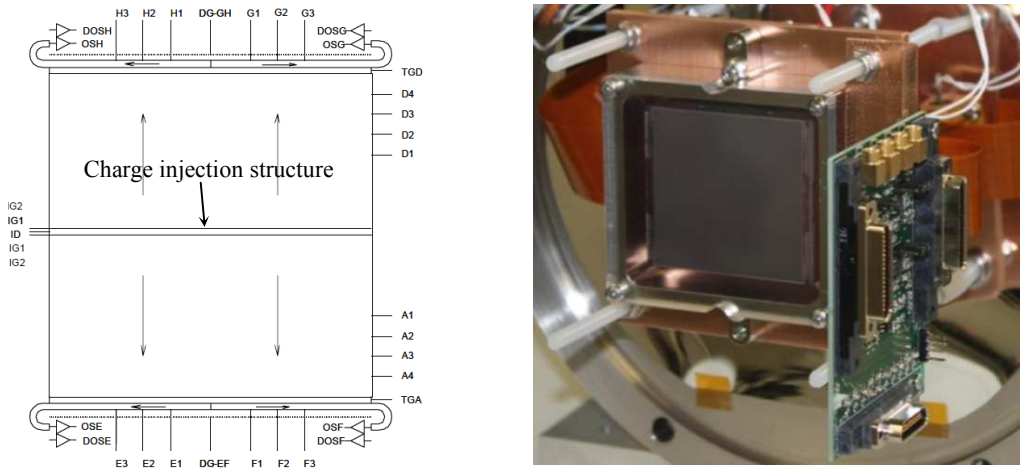

Figure 4. Schematic and photograph of the e2v technologies CCD273, the photograph shows the CCD273 mounted onto a copper cold bench as part of the CEI test camera.

Table 1. Details on the CCD203, CC204 and CCD273.

Parameter	CCD203	CCD204	CCD273
Number of pixels	4136 (V) × 4096 (H)	1064 (V) × 4096 (H)	4132 (V) × 4096 (H)
Pixel Size	12 µm square	12 µm square	12 µm square
Prescan (lead-in) pixels	50	50	50
Register channel width	50 µm	50 µm	20 µm
Charge Injection structure	N/A	top of image area	centre of image area

After launch Euclid will take approximately 30 days to enter into an orbit around the second Sun-Earth Lagrange point, L2, where it will operate for 5 to 6 years. During this period the spacecraft will be continually bombarded by charged particles from the space radiation environment, resulting in displacement damage within the CCD detectors. The resulting vacancies drift through the silicon lattice and can combine with other defects to form stable defects, the three main defects for n-channel CCDs are the phosphorus-vacancy (E-centre), the oxygen-vacancy (A-centre) which are the result of impurity atoms in the lattice, and the divacancy (J-centre) consisting of two adjacent vacancies[17]. The lattice defects create energy levels in the silicon band-gap which change the properties of the material through several different processes, including generation, recombination, trapping, tunnelling and scattering[17].

Generation and trapping are the processes which have the greatest impact on CCD operation under irradiation, resulting in increased dark current and increased CTI[18] respectively. The increase in CTI will lead to the introduction of systematic shear measurements, making it beneficial that the effect of radiation-induced CTI in the Euclid CCDs is understood[13]. The current predicted Euclid end of life 10 MeV equivalent proton fluence, calculated using the European Space Agencies SPace ENVironment Information System[19] (SPENVIS) is 4.8×10^{9} protons.cm^{-2}.

This paper describes part of the work performed on an initial radiation damage assessment performed using the CCD273, focussing on the comparison of CTI as a function of proton fluence between the CCD204 and the CCD273. This work was funded by ESA.

2. EXPERIMENTAL ARRANGEMENT

The two CCD273s available for testing were held within the centre for electronic imaging (CEI) Euclid vacuum test facility, illustrated in Figure 5. The CCD under test was clamped onto a copper cold bench, illustrated in Figures 3 and 4 for the CCD204 and CCD273 respectively, connected to a CryoTiger® refrigeration system capable of cooling the CCD to around -130 °C. The temperature was controlled using a feedback system, comprising a Lakeshore 325 temperature controller, platinum resistance thermometer (PRT), and a heater. Two temperature sensors are held within the CCD273 package and a third was mounted onto the copper cold bench. An XTF5011/75-TH X-ray tube was used to fluoresce a polished manganese target held at 45° to the incident X-ray beam to provide around one X-ray event per eighty pixels. Event re-combination code was used to combine split events for the purpose of counting the number of X-rays detected. The manganese target is held at a distance to provide a uniform X-ray exposure at the CCD, and the vacuum bellows allows for minor adjustments to be made. Clocking and biasing was provided by an XCAM ltd. USB2REM2 camera drive box in conjunction with drive software controlled use a custom MatLab software program. The same camera system was used during the data collection of both the CCD204 and CCD273 study.

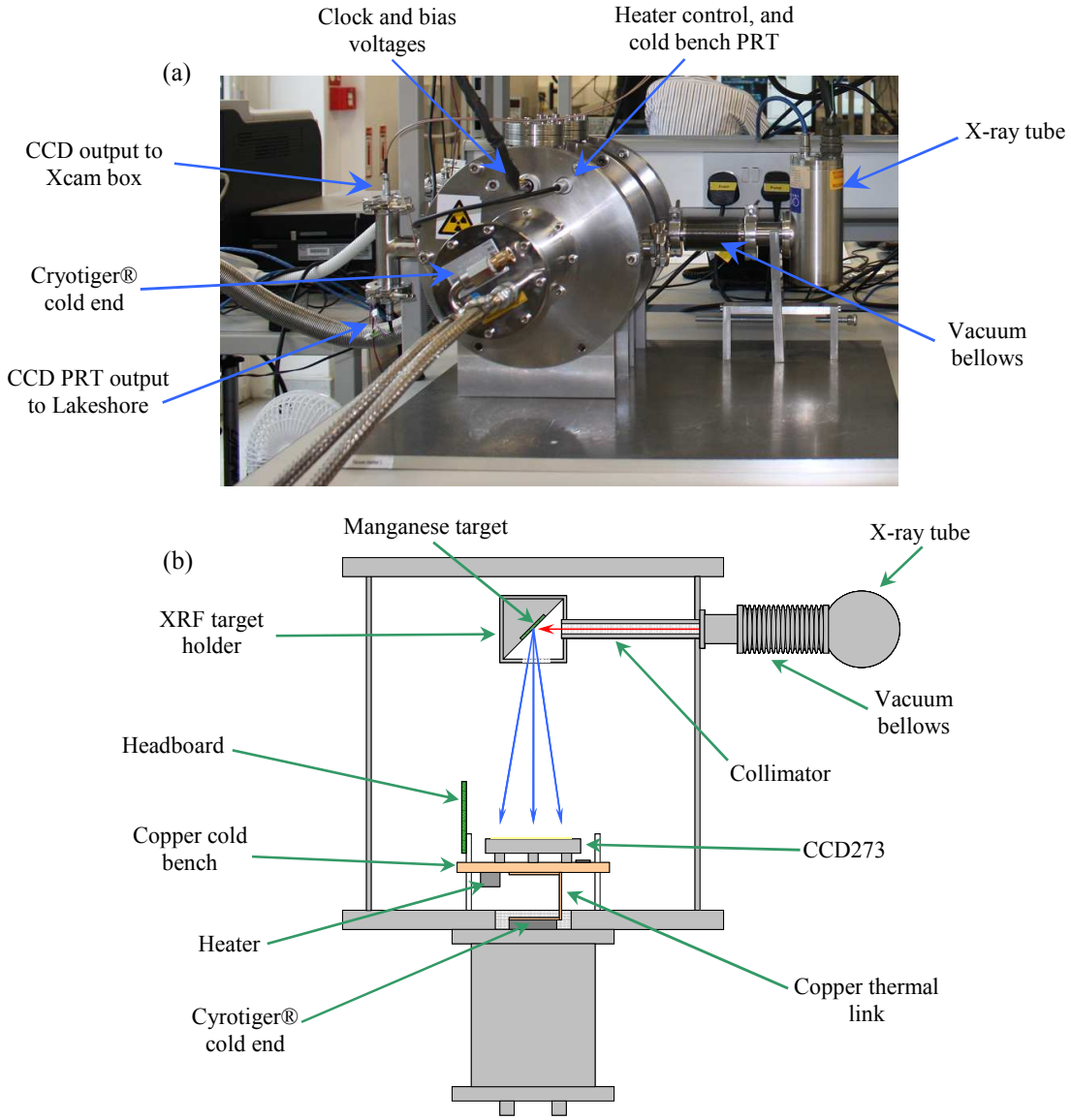

Figure 5. A photograph of the Euclid CCD test chamber (a) and a schematic of the CCD mounted inside the chamber (b)

3. EXPERIMENTAL TECHNIQUE

The CCD204 and CCD273 were both readout at 200 kHz, using the clocking scheme illustrated in Figure 6. Data was collected using an integration time of 500 s and a pause of 90 s between the completion of CCD readout and the next image acquisition, during which time the CCD was continually readout. Further details on the CCD204 testing are available in Gow *et al.* 2012[13]. The number of rows readout to form an image was the same during data collection with the CCD204 and CCD273 to ensure the parallel dwell time remained un-changed.

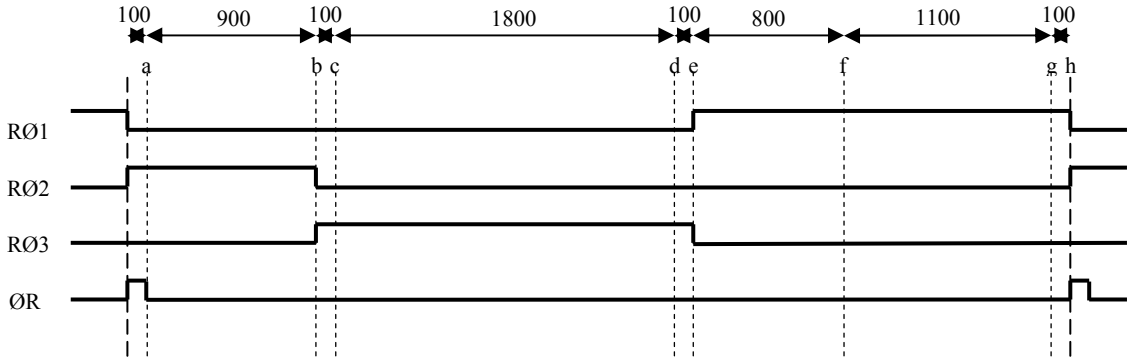

Figure 6. Clocking scheme used for CCD204 and CCD273 readout[13]

CTI measurements were performed using the X-ray technique[20], with the CCD split into bins of 30 pixels for parallel and serial CTI measurements respectively. A peak fitting routine was then used to identify the Mn-Kα peak location within each bin, a line of best fit to these data points can then be used to calculate the CTI. The error on the CTI was calculated using the error on the weighted mean of the peak location and the error on the gradient, found using a parallelogram of error. Only events identified as isolated were used for the analysis, events were selected using a threshold of 6σ in un-irradiated regions and 10σ in the irradiated regions, where σ is the standard deviation of the noise peak. No event reconstruction was performed for the CTI analysis. A scatter plot of X-ray events across the columns of the CCD is illustrated in Figure 7, showing the resulting fit to the data and the effect of charge travelling in the serial direction through a region irradiated with a 10 MeV equivalent proton fluence of 8.0×10^{9} protons.cm^{-2}.

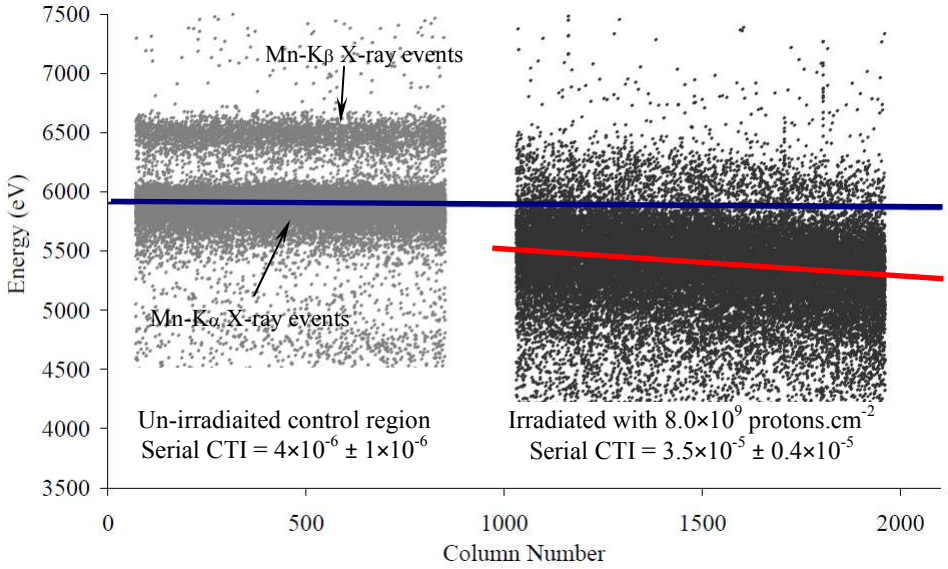

Figure 7. X-ray scatter plot showing the measured energy as a function of column number across a region of a CD273 irradiated with a 10 MeV equivalent proton fluence of 8.0×10^{9} protons.cm^{-2} and held at -113.0 °C.

3.1 Proton Irradiation

The proton irradiation was performed on the two CCD273s available for testing at the Kernfysisch Versneller Instituut (KVI) in Holland using a primary beam of 66 MeV protons, with 50 MeV protons incident onto the CCD at a flux of 2×10^{7} protons.cm^{-2}.s^{-1}. Details on the 10 MeV equivalent proton fluence delivered to each CCD are given in Table 2, with the areas irradiated illustrated in Figure 8. The CCD204 was irradiated using the same beam energy and flux[13], the fluence levels are given in Table 2.

Table 2. Details on the proton irradiation performed at KVI using 50 MeV protons incident on the CCD.

Device	Type	10 MeV equivalent proton fluence (protons.cm^{-2})	
Device 1	CCD204	2.0×10^{9}	4.0×10^{9}
Device 2	CCD204	8.0×10^{9}	Cryogenic Irradiation
Device 3	CCD273	2.0×10^{9}	8.0×10^{9}
Device 4	CCD273	4.8×10^{9}	1.6×10^{10}

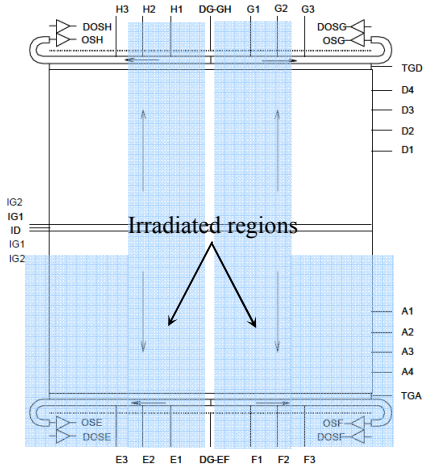

Figure 8. Schematic of the CCD273 showing the irradiated regions.

4. RESULTS AND DISCUSSIONS

The CTI was measured using data collected with the CCD held at -113 °C pre- and post-irradiation. The parallel CTI measured using the CCD204 and CCD273 as a function of proton fluence is illustrated in Figure 9, as would be expected using the same clocking timings and pixel structure produces comparable results. The serial CTI measured as a function of proton fluence is illustrated in Figure 10, showing a clear improvement as a result of the reduction in register volume. The increase in the error on serial measurements is due to the decreased number of transfers, i.e. ~2000 parallel transfers compared to ~800 transfers in the irradiated regions, available for analysis. The radiation damage constant (RDC), given by equation 1

$$RDC = \frac{\Delta CTI}{10\,MeV\ equivalent\ proton\ fluence} \tag{1}$$

was found by fitting a line to the data points for the CCD204 and CCD273 respectively. Comparing the RDC values for the serial CTI of the CCD204 and CCD273, calculated to be 5.8×10^{-15} and 3.5×10^{-15} respectively, the factor of improvement achieved through the reduction in register volume, operating under these conditions, was found to be a factor of 1.7.

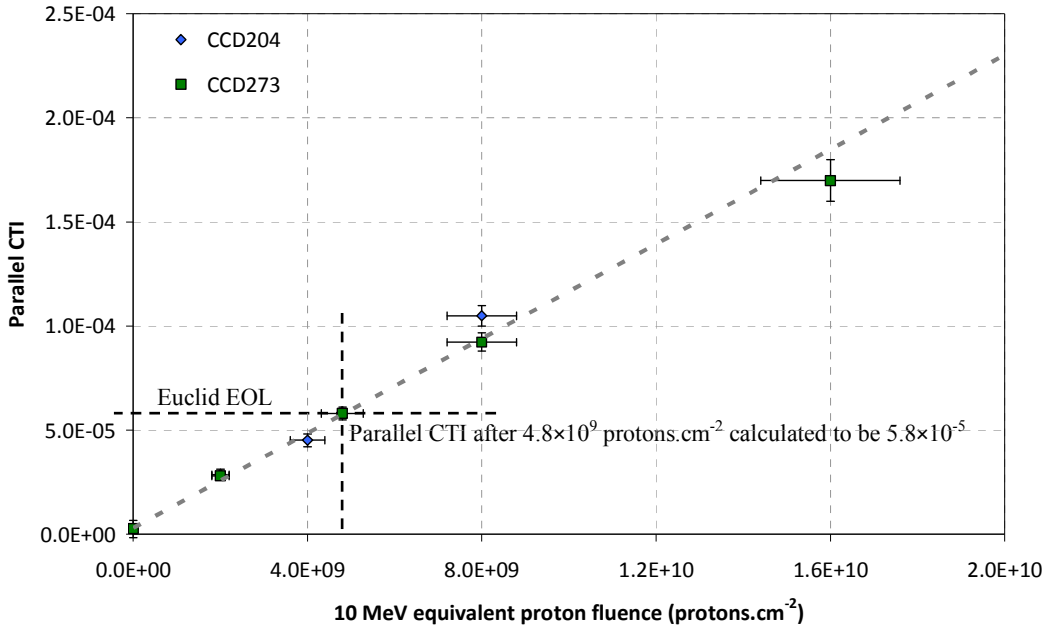

Figure 9. Parallel charge transfer inefficiency as a function of 10 MeV equivalent proton fluence measured using CCD204 and CCD273 detectors showing comparable performance.

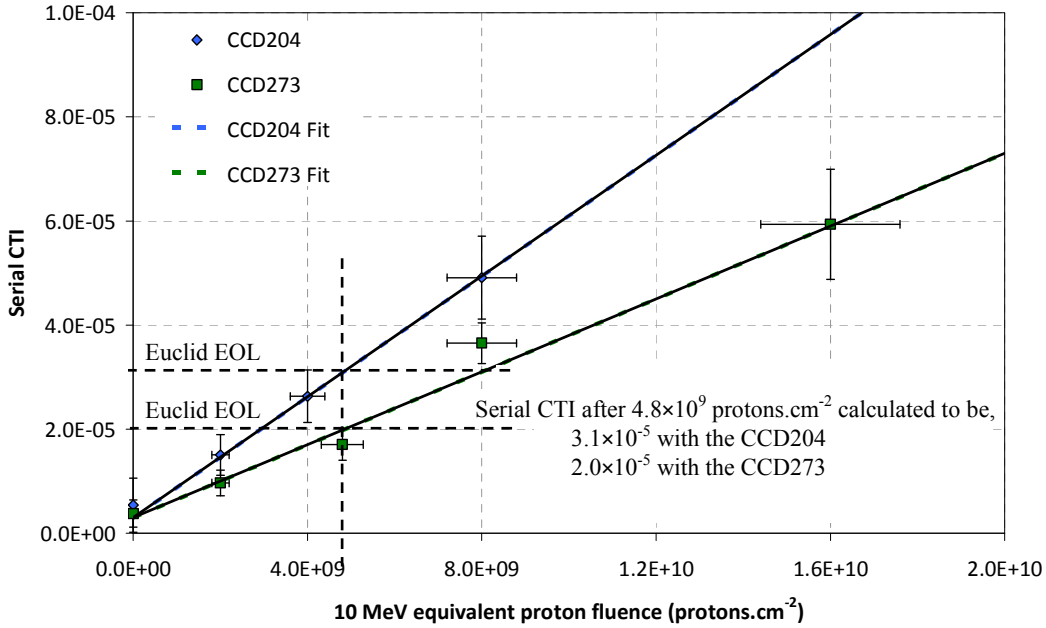

Figure 10. Serial charge transfer inefficiency as a function of 10 MeV equivalent proton fluence measured using CCD204 and CCD273 detectors, where the reduction in register volume in the CCD273 demonstrates an improvement in tolerance to radiation induced serial CTI by a factor of 1.7.

The volume occupied by charge packets consisting of different numbers of electrons was modelled, using Silvaco, for the CCD204 and CCD273 serial registers[14]. Using the assumption that the larger the charge packet the great the number of traps encountered, the relative volume between the CCD204 and CCD273 was calculated as a function of the number of electrons in the charge packet. This provided an indication of the improvement in serial CTI with reduced register volume. At ~1,600 e^- the model predicted an improvement of a factor of ~1.9 in the serial CTI using the reduced volume CCD273 register.

5. CONCLUSIONS

The creation of a custom CCD, in the form of the CCD273, for the Euclid mission is the result of discussion between the Euclid VIS consortium, ESA and e2v technologies to create a CCD designed specifically to meet the specifications of the VIS instrument. The aim of the initial assessment into the effect of proton damage on radiation induced CTI was to analyse the effect of the reduction in register volume, achieved by reducing the channel width from 50 μm to 20 μm, in the CCD273 compared to data collected as part of the Euclid radiation damage study performed using the CCD204. The improvement in tolerance to radiation induced serial CTI in the CCD273 was experimentally measured to be a factor of 1.7 using Mn-Kα X-rays (~1,600 e^-) which compares well to the modelled value of 1.9 found using a charge packet containing ~1,600 e^-. As would be expected the parallel CTI was found to be comparable for both the CCD204 and CCD273, as the same clock timings and pixel structure is used in both CCDs.

The next stage in the model verification will be to perform CTI measurements over a range of charge levels using the extended pixel edge response technique[20], where charge will either be injected using the charge injection structure or provided using a diffuse optical background. This will be performed using both the CCD204 and CCD273 to replicate, experimentally, Figure 4 of Clarke *et al.* 2012[14].

Upon the completion of the work involved in the initial radiation damage assessment of the CCD273 the dark current will be measured as a function of temperature, bright defects identified to be exhibiting greater than 300 $e^-.pix^{-1}.min^{-1}$ at 173 K identified, the range and uniformity of the charge injection structure assessed and the CTI measured using Euclid appropriate operating conditions over the nominal CCD operating range.

Work will also continue on developing clocking schemes to minimise the impact of trapping on both parallel[21] and serial CTI. The use of an even clocking scheme (all clocks high for the same period) demonstrated a factor of 1.2 improvement in RDC for serial CTI over the scheme illustrated in Figure 5[15]. Assuming the improvement is comparable for the CCD273 the serial CTI after 4.8×10^9 protons.cm^{-2} is predicted to be around $1.8\text{x}10^{-5}$ using even mode clocking.

REFERENCES

[1] Zwicky F., "On the Masses of Nebulae and of Clusters of Nebulae," Astrophysical Journal 86, 217 (1937).

[2] Einstein A., "Lens-like Action of a Star by the Deviation of Light in the Gravitational Field," Science 84, 506 (1936).

[3] NASA Hubble Space Telescope Image (1999).

[4] Lynds R. and Petrosian V., "Giant Luminous Arcs in Galaxy Clusters," Bulletin of the American Astronomical Society 18, 1014 (1986).

[5] Soucail G., *et al.*, "Further data on the blue ring-like structure in A 370," Astronomy and Astrophysics vol. 184 , 7-9 (1987).

[6] Rhodes J., *et al.*, "Weak lensing from space I: prospects for the SuperNova/Acceleration Probe," Astropart. Phys., 377 (2004).

[7] Jain B., "Magnification Effects as Measures of Large-Scale Structure," The Astrophysical Journal 580, 3 (2002).

[8] Lumb D., *et al.*, "Euclid Mission – assessment study," Proc. of SPIE vol. 7436, (2009).

[9] Kamionkowski M., *et al.*, "Theory and statistics of weak lensing from large-scale mass inhomogeneities," Mon. Not. R. Astron. Soc. 301, 1064 (1998).

[10] Blake C. and Glazebrook K., "Probing Dark Energy Using Baryonic Oscillations in the Galaxy Power Spectrum as a Cosmological Ruler," The Astrophysical Journal, Vol. 594, 665 (2003).

[11] Cropper M. et al, “VIS: the visible imager for Euclid,” Proc. of SPIE vol. 8442 (2012).

[12] Prieto E. et al, “The Euclid near-infrared spectrophotometer instrument concept at the end of the phase A study,” Proc. of SPIE vol. 8442 (2012).

[13] Gow J. P. D., *et al.*, “Assessment of space proton radiation-induced charge transfer inefficiency in the CCD204 for the Euclid space observatory,” Journal of Instrumentation vol. 7, (2012).

[14] Clarke A. S., *et al.*, “Modelling charge storage in Euclid CCD structures,” Journal of Instrumentation vol. 7, (2012).

[15] Hall D. J, *et al.*, “Optimisation of device clocking schemes to minimise the effects of radiation damage in charge coupled devices,” IEEE Transactions on Electron Devices vol. 59 no. 4, 1099-1106 (2012).

[16] Endicott J., “Charge-coupled devices for the ESA Euclid M-class Mission,” Proc. of SPIE vol. 8453 (2012).

[17] Srour J. R., Marshall C.J., and Marshall P.W., “Review of Displacement Damage Effects in Silicon Devices,” IEEE Trans. Nucl. Sci. vol. 50 issue 3, (2003).

[18] Holland A. D., “The effect of bulk traps in proton irradiated EEV CCDs,” Nuclear Instruments and Methods in Physics Research Section A vol. 326, 335 (1993).

[19] Heynderickx D., *et al*., Proc. AIAA 0371, (2000).

[20] Janesick J. R., “Scientific Charge Coupled Devices,” SPIE Press Washington, (2001).

[21] Murray *et al., “*Mitigating radiation-induced charge transfer inefficiency in full-frame CCD applications by 'pumping' traps,” Proc. of SPIE vol. 8453, (2012).